Polyphosphates diminish solubility of a globular protein and thereby promote amyloid aggregation

Received for publication, March 29, 2019, and in revised form, August 21, 2019 Published, Papers in Press, August 22, 2019, DOI 10.1074/jbc.RA119.008662

Kenji Sasahara, Keiichi Yamaguchi, Masatomo So, and Yuji Goto[1]

From the Institute for Protein Research, Osaka University, 3-2 Yamadaoka, Suita, Osaka 565-0871, Japan

Edited by Paul E. Fraser

Structural changes of globular proteins and their resultant amyloid aggregation have been associated with various human diseases, such as lysozyme amyloidosis and light-chain amyloidosis. Because many globular proteins can convert into amyloid fibrils *in vitro*, the mechanisms of amyloid fibril formation have been studied in various experimental systems, but several questions remain unresolved. Here, using several approaches, such as turbidimetry, fluorescence and CD spectroscopy, EM, and isothermal titration calorimetry, we examined the binding of polyphosphates to hen egg-white lysozyme under acidic conditions and observed polyphosphate-induced structural changes of the protein promoting its aggregation. Our data indicate that negatively charged polyphosphates bind to protein molecules with a net positive charge. The polyphosphate-bound, structurally destabilized protein molecules then start assembling into insoluble amorphous aggregates once they pass the solubility limit. We further show that the polyphosphates decrease the solubility limit of the protein and near this limit, the protein molecules are in a labile state and highly prone to converting into amyloid fibrils. Our results explain how polyphosphates affect amorphous aggregation of proteins, how amyloid formation is induced in the presence of polyphosphates, and how polyphosphate chain length is an important factor in amyloid formation.

Protein aggregation is a complex process and resultant aggregates can differ in morphology, from soluble or highly ordered oligomers to insoluble amorphous aggregates or amyloid fibrils (1, 2). Amyloid fibrils, which are highly ordered filamentous assemblies, possess a core structure of extended cross-β-sheets, in which individual β-strands are perpendicular to the fibril axis (3). Growing evidence has pointed to the toxic potential of oligomeric states and/or intermediates formed during fibril formation, and to their involvement in cellular dysfunction in amyloid-related diseases (4, 5). In contrast to nucleation-dependent growth of amyloid fibrils, which occurs with a lag time (6), amorphous aggregation, in which various assemblies without organized intermolecular interactions are formed, is generally rapid and occurs without a detectable lag phase (7–10). Amorphous aggregation is associated with the development of cataracts (11) and precipitation of recombinant proteins during their expression and purification (12). Several amyloidogenic proteins can form both types of aggregates *in vitro*, competing both kinetically and thermodynamically in the aggregation process (8–10, 12–16). However, neither the role played by amorphous aggregation in amyloid fibril formation, nor the molecular mechanisms underlying amyloid fibrillation, are fully understood.

In the conversion to amyloid fibrils, the conformational stability of globular proteins and their solubility in aqueous solution are assumed to be important factors (17, 18). In most cases, amyloid fibrils and amorphous aggregates are formed in physiological solutions when the properties of the surrounding solvent, such as the solution pH, temperature, type and concentration of salts, and presence of additives, destabilize the native conformation of the proteins in solutions (8–10, 18–20). The solubility of globular proteins is determined by their amino acid content, the pK_a values of the ionizable residues, the protein conformational states, and environmental factors such as pH, temperature, salt type, and salt concentration (21). In defining the phase diagram of a protein's aggregation, determining its solubility curve is essential (10, 22). Interestingly, recent studies have shown that the concentrations of proteins in the cell are typically close to their solubility limit, suggesting that many proteins *in vivo* are exposed to risk of aggregation under stress or due to aging (23–25). How decreased solubility and stability of globular proteins affect their propensity to convert into fibrillar structures remains an unclarified issue that may be crucial to understanding amyloid fibril formation *in vivo*.

In this context, polyanions, such as ATP, DNA, heparan sulfate, and polyphosphate, are important variables affecting protein stability and solubility (26–31). Many low-molecular weight salts, for example, NaCl, Na_3PO_4, and Na_2SO_4, affect protein aggregation in diverse ways, such as the Hofmeister effect (32–34), preferential interactions (33, 35), and specific binding (36, 37). Compared with salt-associated protein aggregation, the polyanions described above were found to dramatically increase the aggregation of amyloidogenic proteins and stabilize the resultant aggregates, in a manner significantly dependent on the net charge and size of the polyanions (26–31, 38). However, the specific nature of the interactions involved in amorphous aggregation and amyloid fibril formation is not fully

This work was supported by Cooperative Research Program for the Institute for Protein, Osaka University, Grants CR-15-02 and ICR-16-02, and JSPS KAKENHI Grants 15H04362, 17K07363, and 17K15074, and MEXT KAKENHI Grants 16H00836 and 17H06352, JSPS Core-to-Core Program A (Advanced Research Networks), and the SENTAN from the Japan Agency for Medical Research and Development (AMED). The authors declare that they have no conflicts of interest with the contents of this article.
This article contains Figs. S1–S8.

[1] To whom correspondence should be addressed. Tel.: 81-6-6879-8614; Fax: 81-6-6879-8616; E-mail: gtyj8126@protein.osaka-u.ac.jp.

understood. Here, under acidic conditions, we investigated the effects of polyphosphates on the aggregation of a globular protein, hen egg-white lysozyme (HEWL),[2] focusing on the decrease in stability and solubility of the protein.

HEWL, comprising 129 amino acid residues, is a basic protein with isoelectric point (pI) of ~11.2 and a net charge of +19 at pH < 3 that forms well-defined amyloid fibrils under acidic conditions (39, 40). The protein has a structure highly homologous to human lysozyme, which forms amyloid fibrils in individuals suffering from hereditary nonneuropathic systemic amyloidosis (also known as lysozyme amyloidosis) (39).

Phosphate is essential for life. It accumulates in cells as polyphosphate, which is a linear polymer of P_i linked by phosphoanhydride bonds (41, 42). Interestingly, recent studies have revealed that polyphosphates promote amyloid fibril formation of several amyloidogenic proteins (30, 38), whereas another study showed inhibition of protein aggregation, in which polyphosphates played a chaperon-like role (43). However, little is known about the mechanisms by which polyphosphates promote or inhibit amyloid fibril formation.

We examined the binding of polyphosphates to HEWL molecules, the resultant structural changes of the protein, and subsequent protein aggregation using turbidimetry, fluorescence, and circular dichroism (CD) spectroscopy, transmission electron microscopy (EM), and isothermal titration calorimetry (ITC). Our results offer a model in which protein aggregation is modulated by binding of polyphosphate molecules.

Results

To assess the ability of negatively charged phosphate groups in a linear chain linked by phosphoanhydride bonds to promote aggregation of positively charged HEWL, we first tested three different sodium phosphates in acidic solution containing 10 mM HCl (pH 2): pyrophosphate (Pyro-P), tripolyphosphate (Tri-P), and tetrapolyphosphate (Tetra-P). Turbidity assays were used to detect protein aggregation in each solution. The concentration of HEWL was 1.0 mg/ml (70 μM), and concentrations of the phosphates varied from 0 to 1.0 mM, where molarity of the polyphosphate species was used as the phosphate concentration. After mixing the respective solutions (that is, HEWL, HCl, and phosphates) and incubating for 1 h at room temperature, turbidity of the solutions was recorded as the apparent absorbance at 600 nm. No significant increases in the turbidity were observed when Pyro-P and Tri-P were used at any of the concentrations tested (Fig. S1). However, as seen in Fig. 1*A*, the turbidity of the solutions increased greatly in the presence of Tetra-P. The same measurements were conducted for protein concentration of 0.2 mg/ml, and the turbidity similarly increased until reaching a plateau (Fig. 1*B*). In Fig. 1, *A* and *B*, the turbidity data are plotted against the logarithmic concentration of Tetra-P, showing the solution turbidity increasing at a certain Tetra-P concentration (~0.1 mM). These data suggest that under the conditions used, two or three phosphate groups are insufficient to cause protein aggregation, and the aggregation-inducing capacity of Tetra-P arises from its longer polymeric nature.

Similar experiments were conducted to examine the effects of NaCl on protein aggregation induced by Tetra-P. Here, the electrostatic shielding effect of NaCl was expected to suppress Tetra-P–induced protein aggregation. 2.0 M NaCl was added at various ratios into several turbid HEWL–Tetra-P solutions. In these preparations, concentrations of the protein and Tetra-P were maintained at a constant level after the addition of NaCl; the final concentrations were 1.0 and 0.2 mg/ml of HEWL, and 1.0, 0.5, and 0.2 mM Tetra-P. The turbidity measurements were similarly conducted after 1 h of incubation at room temperature (see Fig. 1, *C* and *D*, for the protein solutions at 1.0 (*C*) and 0.2 mg/ml (*D*), which contained 1.0 mM Tetra-P). For all the protein–Tetra-P solutions studied, the turbidity decreased with increases in NaCl concentration, resulting in transparent solutions (*i.e.* zero turbidity) at concentrations of more than 0.3–0.4 M NaCl (Fig. 1, *C* and *D*, and Fig. S2, A, *C*, and *E*). These results suggest that in Tetra-P–induced aggregation of HEWL, electrostatic interactions are predominantly involved.

We examined the amyloidogenic propensity of these solutions at various NaCl concentrations by adding an amyloid-sensitive dye, thioflavin T (ThT), at 5 μM into several HEWL–Tetra-P–NaCl solutions in which the concentrations of the protein and Tetra-P were maintained at constant levels. The concentrations of NaCl in these solutions are indicated by *arrows* (Fig. 1, *C* and *D*, and Fig. S2, *A*, *C*, and *E*). These 10-set sample solutions at different NaCl concentrations were subjected to repeated ultrasonic irradiation and changes in ThT fluorescence were measured during the intermittent sonication (Fig. S3). Interestingly, upon ultrasonic irradiation, the solutions containing 0.3–0.4 M NaCl exhibited a marked increase in ThT fluorescence after a lag time of ~4–8 h (Fig. 1, *E* and *F*, Fig. S2, *B*, *D*, and *F*, and Fig. S4, *A*–*E* for the time-dependent data of all the samples). For the solutions at concentrations lower and higher than 0.3–0.4 M NaCl, the increase in ThT fluorescence was largely suppressed. These results indicate that ultrasonication triggered amyloid aggregation of the protein molecules in the vicinity of their solubility limit. CD spectra of these solutions were recorded after the ThT fluorescence measurements were taken (Fig. 1*G*). The CD data clearly indicated the formation of β-sheet structures, characterized by a peak around 220 nm, for the solutions that showed high ThT fluorescence (Fig. 1*F*). EM images obtained for these samples confirmed the formation of fibrillar aggregates (Fig. 1, *H* and *I*).

We then investigated the effects of longer polyphosphates, with 10–15 phosphate groups (S-PolyP) and with 60–70 phosphate groups (L-PolyP), on protein aggregation. The same turbidity measurements as shown in Fig. 1, *B* and *D*, were conducted. The turbidity of the solutions containing S-PolyP or L-PolyP increased at lower concentrations of the polyphosphates as the chain lengths became longer (Fig. 2, *A* and *B*). Addition of NaCl to the turbid solutions containing S-PolyP and L-PolyP resulted in decreased turbidity as NaCl concentration increased (Fig. 2, *C* and *D*). The turbidity reached 0 at NaCl concentrations around 0.6–0.8 M, which were larger values

[2] The abbreviations used are: HEWL, hen egg-white lysozyme; Tetra-P, sodium tetrapolyphosphate; Tri-P, sodium tripolyphosphate; Pyro-P, sodium dihydrogen pyrophosphate; S-PolyP, short polyphosphate; L-PolyP, long polyphosphate; ITC, isothermal titration calorimetry; ThT, thioflavin T.

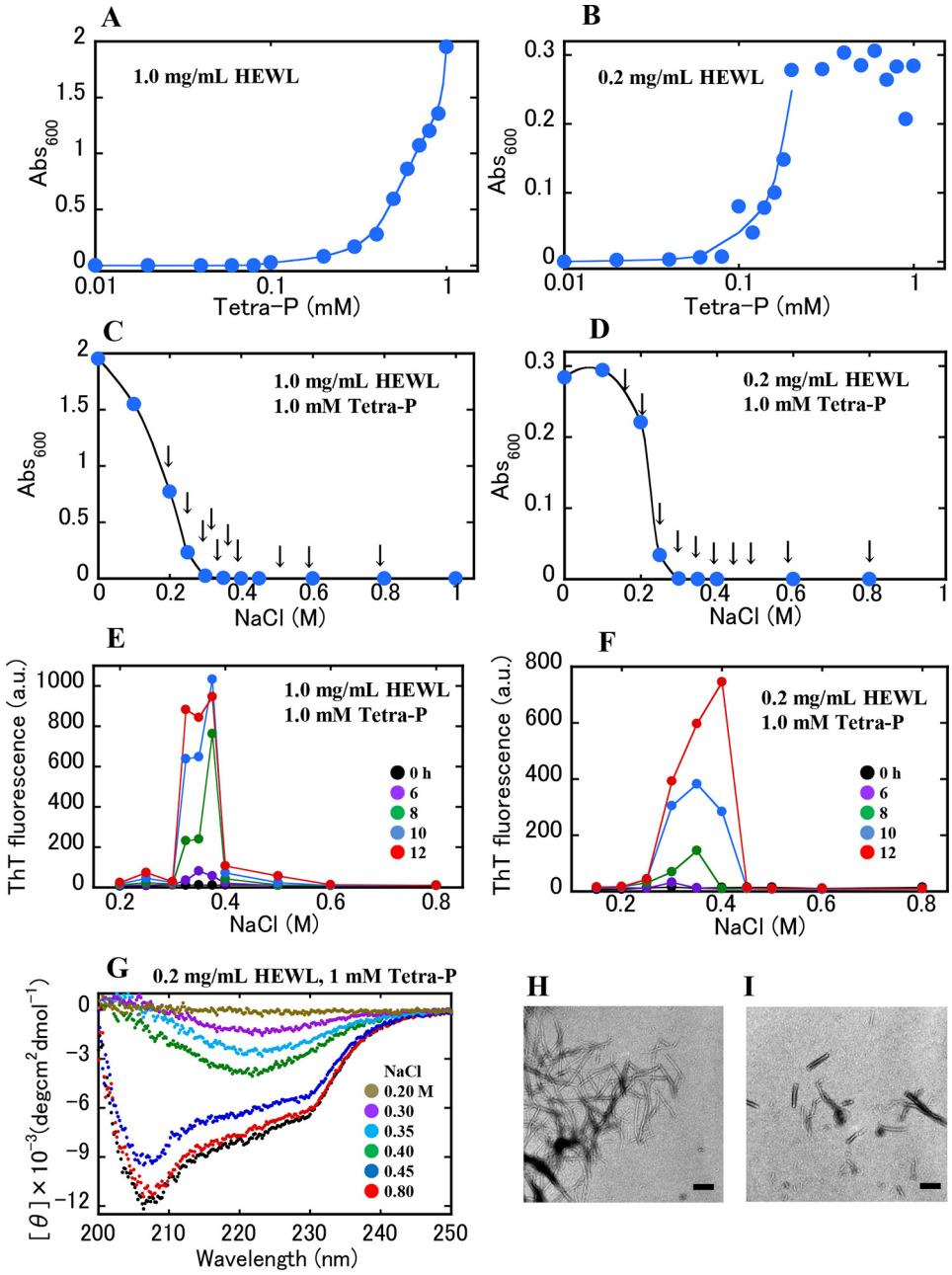

Figure 1. Aggregation of HEWL in the presence of Tetra-P. *A* and *B*, dependence of Tetra-P concentration on solution turbidity. The solutions contained 10 mM HCl, Tetra-P at various concentrations, and HEWL at 1.0 (*A*) and 0.2 mg/ml (*B*). *Curves* were drawn manually along the increasing data points without fitting. *C* and *D*, effects of NaCl on protein aggregation in the presence of 1.0 mM Tetra-P. The protein concentrations were 1.0 (*C*) and 0.2 mg/ml (*D*). *Curves* were drawn manually along the data points. The 10 *arrows* indicate the NaCl concentrations of the samples used in the sonication-induced aggregation experiments (see below). In *A–D*, the samples were incubated at room temperature for 1 h before turbidity assay. *E* and *F*, sonication-induced aggregation. The data in *E* and *F* were obtained from the 10 samples at different NaCl concentrations denoted by the *arrows* in *C* and *D*, respectively. Fluorescent measurements were performed every 2 h during incubation at 37 °C: 0, 2, 4, 6, 8, 10, and 12 h (see Fig. S4, *A* and *D*). Data recorded during incubation for 0, 6, 8, 10, and 12 h are shown in the figures. *G*, CD spectra of sonication-treated samples in *F*. The concentrations of NaCl in the sample solutions are shown. The *black-filled circles* represent the control sample (HEWL in the solution containing 0.8 M NaCl and 10 mM HCl without Tetra-P). *H* and *I*, EM images. Images *H* and *I* were obtained from both samples at NaCl 0.35 M in *E* and *F*, respectively. *Scale bars* represent 200 nm.

than those (*i.e.* 0.3–0.4 M) detected for Tetra-P. These results suggest that electrostatic attraction between polyphosphate and HEWL becomes stronger with increasing chain lengths.

The 10-set samples containing NaCl at different concentrations, which are indicated by *arrows* in Fig. 2, *C* and *D*, were subjected to ultrasonic irradiation, and changes in ThT fluorescence were recorded (Fig. 2, *E* and *F*). The solutions containing 0.3–0.7 M NaCl exhibited significant increases in ThT fluorescence (Fig. 2, *E* and *F*). The formation of β-sheet structures was observed by CD spectroscopy for some samples showing high ThT fluorescence (Fig. 2, *G* and *H*). EM images confirmed the formation of fibrillar aggregates (Fig. 2, *I* and *J*). The results in Figs. 1 and 2 indicate that when the protein molecules were near their solubility limit, modulated by polyphosphates, amyloid formation was effectively triggered by sonication.

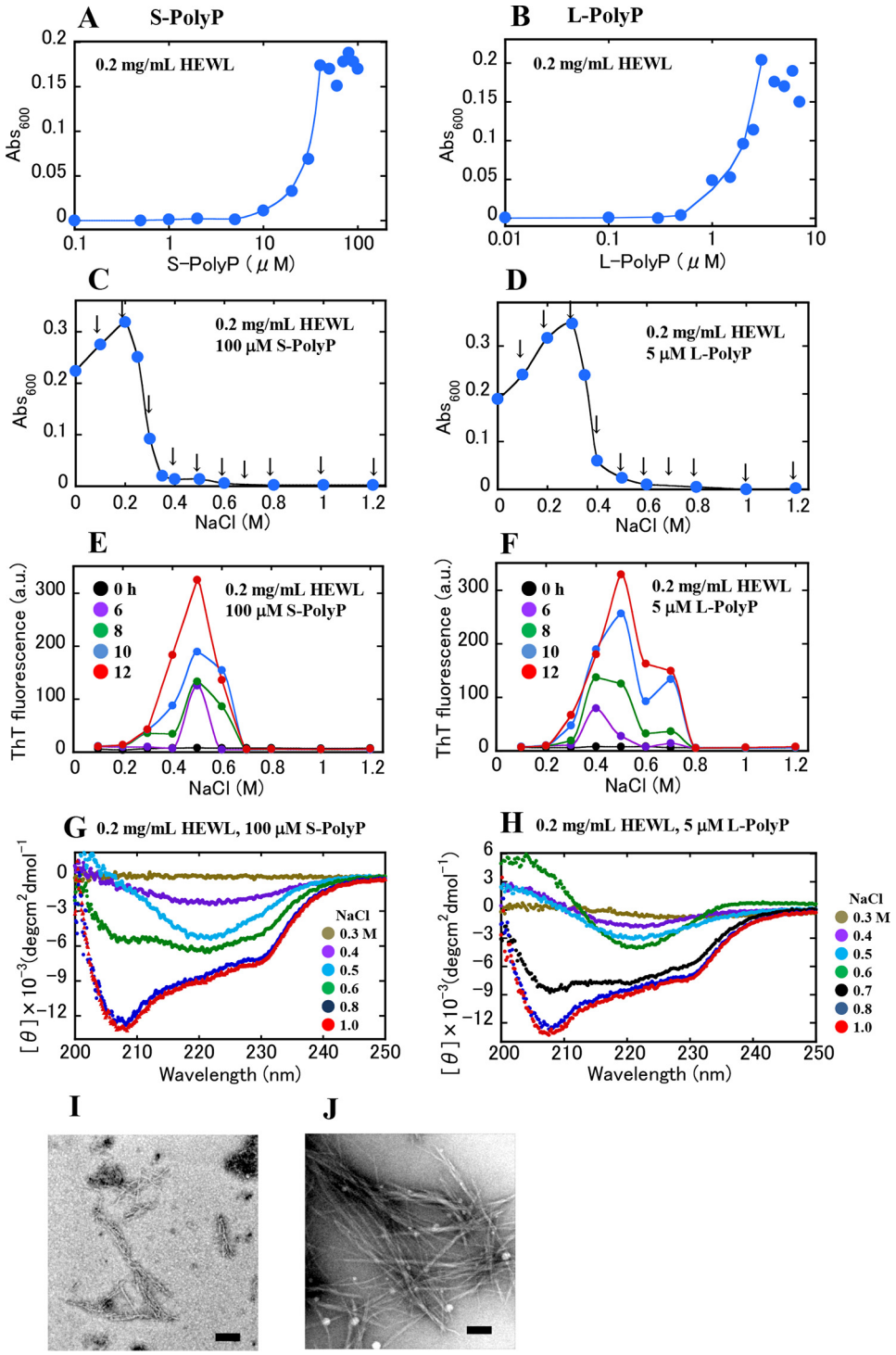

Figure 2. Aggregation of HEWL in the presence of S-PolyP or L-PolyP. *A* and *B*, dependence of polyphosphate concentration on solution turbidity. The solutions contained 0.2 mg/ml of HEWL, 10 mM HCl, S-PolyP (*A*) or L-PolyP (*B*) at various concentrations. *Curves* were drawn along the increasing data points without fitting. *C* and *D*, dependence of NaCl concentration on protein aggregation. The protein solutions (0.2 mg/ml) contained 100 μM S-PolyP (*C*) or 5 μM L-PolyP (*D*), and NaCl at several concentrations. *Curves* were drawn manually along the data points. The 10 *arrows* indicate the NaCl concentrations of the samples that were used in the sonication-induced aggregation experiments. In *A–D*, the samples were incubated at room temperature for 1 h before turbidity assay. *E* and *F*, sonication-induced aggregation. The data in *E* and *F* were obtained from the 10 samples at different NaCl concentrations denoted by the *arrows* in *C* and *D*, respectively. Fluorescent measurements were performed as shown in Fig. 1, *E* and *F* (see Figs. S4, *F* and *G*). *G* and *H*, CD spectra of sonication-treated samples. The spectra in *G* and *H* were obtained from the samples shown in *E* and *F*, respectively. The concentrations of NaCl in the sample solutions are shown in the figures. *I* and *J*, EM images. Images *I* and *J* were obtained from the samples at 0.5 M NaCl in *E* and *F*, respectively. *Scale bars* represent 200 nm.

As the solubility of HEWL was largely modulated by the additions of polyphosphates and NaCl (Figs. 1 and 2), the effects of these additives on the secondary structure of the protein were examined by CD spectroscopy. After preparing several solutions of HEWL and Tetra-P according to the compositions and concentrations shown in Fig. 1*B*, CD spectra of these solutions

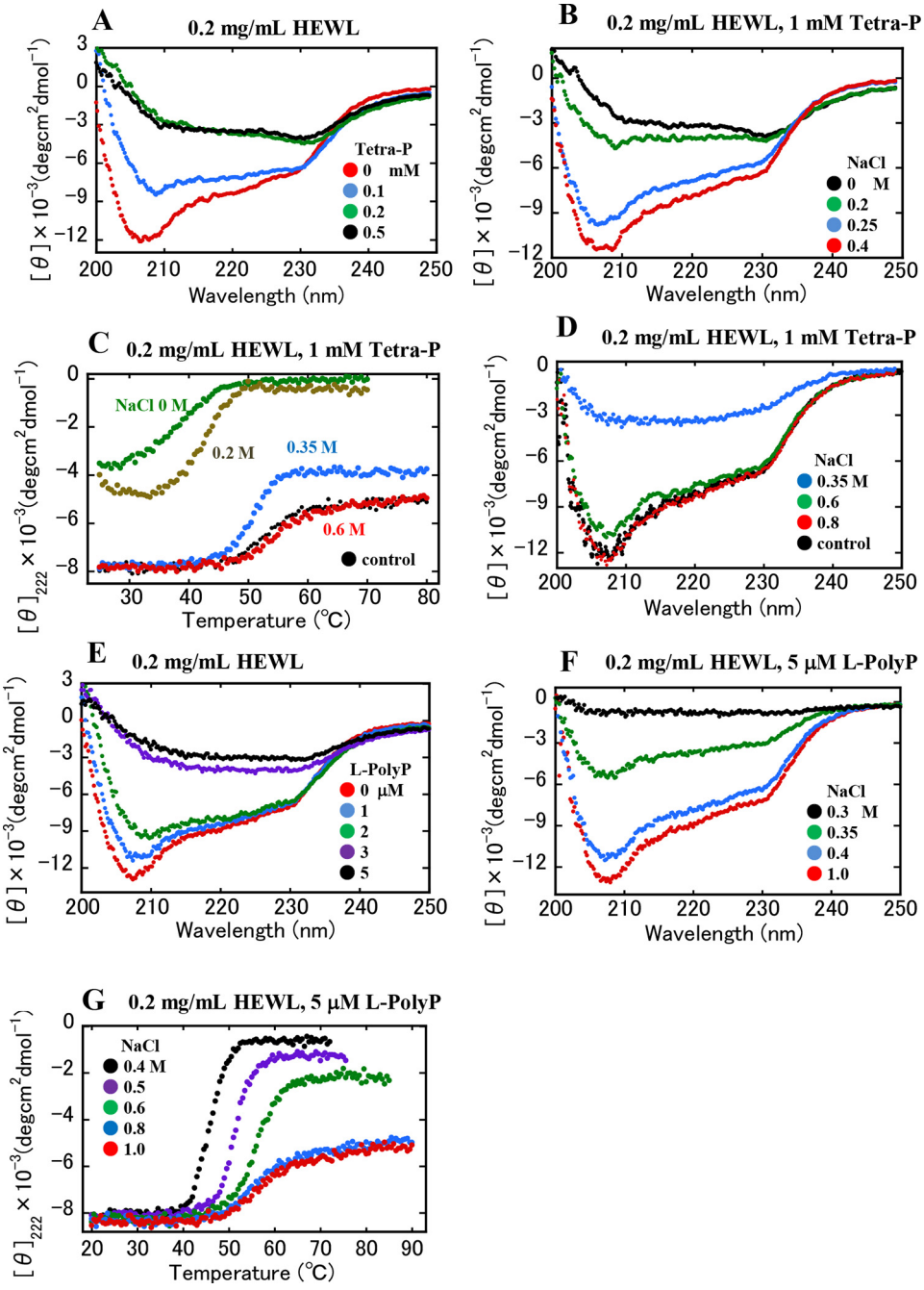

Figure 3. Effects of polyphosphate and NaCl on the structural stability of HEWL (0.2 mg/ml). *A*, CD spectra of HEWL in solutions containing 10 mM HCl and Tetra-P at several concentrations: 0, 0.1, 0.2, and 0.5 mM. *B*, CD spectra of HEWL in solutions containing 10 mM HCl and 1.0 mM Tetra-P and NaCl at various concentrations: 0, 0.2, 0.25, and 0.4 M. *C*, thermal stability of HEWL in the solutions. The protein solutions contained 10 mM HCl, 1.0 mM Tetra-P, and NaCl at several concentrations: 0, 0.2, 0.35, and 0.6 M, and control sample: protein solution at 10 mM HCl without Tetra-P and NaCl. The sample solutions were heated at 1 °C/min. *D*, CD spectra of the sample solutions in *C* after cooling to 25 °C. The samples containing NaCl at various concentrations were heated and cooled; 0.35, 0.6, and 0.8 M NaCl, and control sample. *E*, CD spectra of HEWL in solutions containing 10 mM HCl and L-PolyP at several concentrations: 0, 1.0, 2.0, 3.0, and 5.0 μM. *F*, CD spectra of HEWL in solutions containing 10 mM HCl and 5 μM L-PolyP and NaCl at various concentrations: 0.3, 0.35, 0.4, and 1.0 M. *G*, thermal stability of HEWL in the solutions. The solutions contained 10 mM HCl, 5 μM L-PolyP, and NaCl at several concentrations: 0.4, 0.5, 0.6, 0.8, and 1.0 M. The sample solutions were heated at 1 °C/min. All the sample solutions were incubated at room temperature for 1 h before the CD measurements.

were recorded after 1 h of incubation (Fig. 3*A*). The results indicated that as the protein solutions became turbid with increasing concentrations of Tetra-P, the secondary structure of the proteins was largely disrupted. Similarly, according to the solution preparation shown in Fig. 1*D*, NaCl was added to the turbid protein–Tetra-P solutions (Fig. 3*B*). As NaCl concentrations increased, the previously turbid solutions became transparent and CD spectra indicated a recovery of protein structure. These results indicate that Tetra-P–induced aggregation was accompanied by structural disruption of protein molecules and the original state was restored upon addition of NaCl.

Thermal stability of the protein solutions (0.2 mg/ml) containing 10 mM HCl, 1 mM Tetra-P, and NaCl at several concentrations, was examined by CD spectroscopy. Fig. 3*C* shows the

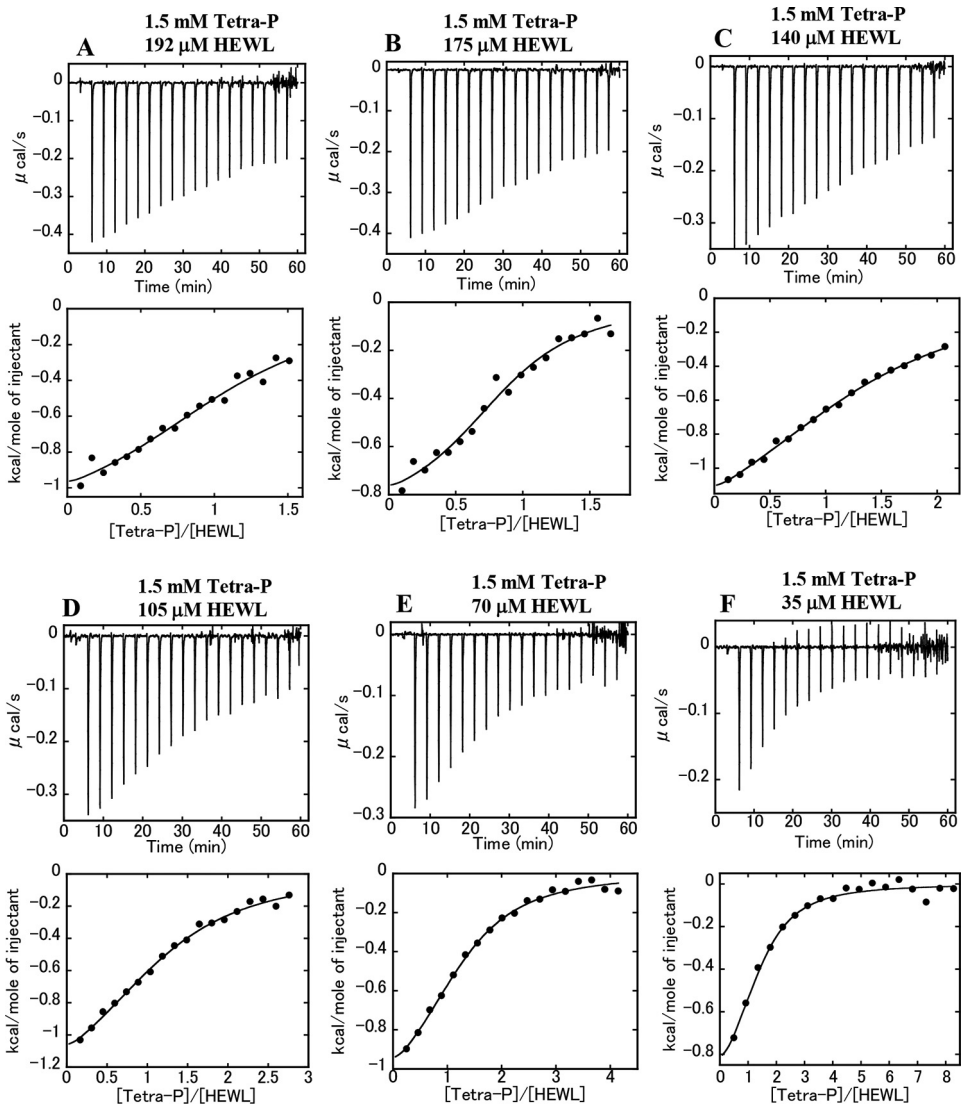

Figure 4. Binding of Tetra-P to HEWL at 25 °C. *A–F*, ITC profiles for titration of Tetra-P into the protein solutions. *Upper panels*: raw data for titration. The Tetra-P solution at 1.5 mM in the injection syringe was titrated into the protein solutions at various concentrations in the ITC cell: 192 (*A*), 175 (*B*), 140 (*C*), 105 (*D*), 70 (*E*), and 35 μM (*F*). 18 injections of 2 μl were carried out. The final concentration of Tetra-P in the cell was 0.24 mM, and those of HEWL were 162 (*A*), 148 (*B*), 118 (*C*), 89 (*D*), 59 (*E*), and 30 μM (*F*). *Lower panels*, integrated heat profile of the calorimetric titration shown in *upper panels*. The integrated heat was plotted against the molar ratio, [Tetra-P]/[HEWL]. The *solid lines* represent the best nonlinear least-squares fit to a single set of binding site model. All the solutions in the syringe and cell contained 10 mM HCl.

temperature-dependent CD intensity at 222 nm for these samples. The turbid solutions at 0 and 0.2 M NaCl showed a deposition behavior of protein during the heating process. At 0.35 M NaCl, near the protein solubility limit, the protein showed an aggregation behavior at higher temperatures. The solution at 0.6 M NaCl showed a typical thermal denaturation curve similar to that of the control sample without Tetra-P. After cooling the samples to 25 °C, their spectra were again recorded (Fig. 3*D*), which confirmed that thermal stabilization of the proteins depends on NaCl concentration.

Similarly, the effects of L-PolyP and NaCl on protein secondary structure were examined by CD spectroscopy. As shown in Fig. 3, *E* and *F*, very similar results were obtained; the secondary structure of the protein was largely disrupted with increasing concentrations of L-PolyP, and the addition of NaCl restored the secondary structure. The temperature-dependent changes in CD intensity at 222 nm were recorded for the HEWL–L-PolyP solutions containing NaCl at 0.4–1.0 M (Fig. 3*G*). The protein in solution at 0.4–0.6 M NaCl, near its solubility limit, showed aggregation at higher temperatures. The protein solutions at 0.8 and 1.0 M NaCl showed typical thermal denaturation curves. These CD data indicate that in the labile state near the solubility limit modulated by Tetra-P and L-PolyP, the protein molecules are structurally destabilized and prone to partially unfolded states, resulting in efficient conversion into amyloid fibrils under ultrasonic irradiation.

ITC measurements were conducted to determine the thermodynamic parameters (ΔG_{bind}, ΔH_{bind}, and ΔS_{bind}) for the binding of Tetra-P to the protein under acidic conditions (10 mM HCl). Calorimetric titrations of Tetra-P into the protein solutions at various concentrations (35–192 μM: 0.5–2.75 mg/ml) were performed at 25 °C (Fig. 4, *A–F*, *upper panels*). Each peak in the binding isotherm represents a heat change associated with a single injection, resulting in exothermic

Table 1
Thermodynamic parameters of the binding of Tetra-P to HEWL at 25 °C

HEWL in the cell[a]	K_D	n	ΔG_{bind}	ΔH_{bind}	$-T\Delta S_{bind}$
	M			*kcal/mol*	
192.0	$54.5\ (\pm 50.2) \times 10^{-6}$	1.12 (±0.37)	−5.8	−1.2 (±0.6)	−4.6
175.0	$26.8\ (\pm 14.9) \times 10^{-6}$	0.86 (±0.09)	−6.2	−0.9 (±0.2)	−5.3
140.0	$79.8\ (\pm 30.6) \times 10^{-6}$	1.33 (±0.15)	−5.6	−1.6 (±0.3)	−4.0
105.0	$49.8\ (\pm 16.6) \times 10^{-6}$	1.17 (±0.07)	−5.9	−1.5 (±0.3)	−4.4
70.0	$28.1\ (\pm 7.0) \times 10^{-6}$	1.19 (±0.06)	−6.3	−1.3 (±0.2)	−5.0
35.0	$17.1\ (\pm 6.2) \times 10^{-6}$	1.19 (±0.15)	−6.5	−1.2 (±0.3)	−5.3

[a] The concentration of Tetra-P in the syringe cell was 1.5 mM.

peaks. The heat resulting from the Tetra-P dilution (that is, titration of the Tetra-P solution into the buffer solution) was very low compared with the heat change associated with the Tetra-P–protein interaction. The integration of each peak, representing the heat-liberated per injection, was plotted against the molar ratio of Tetra-P to the protein (Fig. 4, *A–F*, *lower panels*). The experimental data were fitted to a single set of binding site models to determine the thermodynamic parameters. The parameters, ΔG_{bind} of −5.6 to −6.5 kcal/mol, ΔH_{bind} of −0.9 to −1.6 kcal/mol, and the entropic contribution $-T\Delta S_{bind}$ of −4.0 to −5.3 kcal/mol, were determined for each titration experiment (Table 1). These thermodynamic parameters were plotted against the initial concentrations of HEWL in the ITC cell before the titrations (Fig. 5*A*). The very low dependence of the parameters on protein concentration strongly suggests that these parameters reflect the thermodynamics of the binding reactions between HEWL and Tetra-P. That is, the heat released in the binding reactions represents the involvement of electrostatic interactions, in which negatively charged Tetra-P molecules bind to sites composed of positively charged amino acid residues. Nevertheless, it is important to note that the binding of Tetra-P to HEWL was driven primarily by entropy, with a dissociation constant K_D of 17–80 μM, in which approximately one molecule of Tetra-P was required to bind to one molecule of protein (stoichiometry n: 0.8–1.4, Table 1).

The bindings of S-PolyP and L-PolyP to HEWL were similarly examined under acidic conditions by ITC. The titrations of S-PolyP or L-PolyP into the protein solutions showed saturating titration curves, with the strength of the interactions for S-PolyP and L-polyP being stronger than that for Tetra-P (Fig. S5). The thermodynamic parameters for binding were determined and plotted against the initial concentrations of HEWL in the ITC cell (Fig. 5, *B* and *C*). The results indicate that enthalpy of binding is favorable for both S-PolyP and L-PolyP, in contrast to Tetra-P. The enthalpy-driven reaction indicates that stronger electrostatic interactions play a major role in the overall binding process, probably due to the higher charge densities of S-PolyP and L-PolyP *versus* Tetra-P. It is noteworthy that more significant changes in enthalpy (ΔH_{bind}) and entropy ($-T\Delta S_{bind}$) were observed for the interaction between HEWL and L-PolyP, compared with Tetra-P and S-PolyP.

Additionally, the binding reactions of Tri-P and Pyro-P to HEWL were examined by ITC (Fig. S6, *A–D*). Exothermic binding was observed for the titration of Tri-P, and fitted to the same binding model, but the heat changes were smaller than for Tetra-P (Fig. S6, *A* and *B*). Importantly, the exothermic heat changes detected for the titration of Pyro-P were too small to fit to the model (Fig. S6, *C* and *D*). As a result, the calorimetric data indicate that the binding affinities of polyphosphates for HEWL depend on their chain lengths: L-PolyP > S-PolyP > Tetra-P > Tri-P > Pyro-P.

As shown in Figs. 1 and 2, increased protein aggregation, as determined by an increase in solution turbidity, was induced at higher concentrations of polyphosphates. To evaluate the heat associated with Tetra-P–induced protein aggregation by ITC, protein solutions at 0.35, 0.49, and 0.7 mM (10 mg/ml) were titrated into a Tetra-P solution at 1.0 mM, conditions under which the solution became turbid (see Fig. S8*A*). Compared with titration of the buffer solution (10 mM HCl) into the Tetra-P solution, noticeable exothermic heat associated with protein aggregation was observed (Fig. 6, *A–C*, *upper panels*). The heat released per injection was plotted as a function of the molar ratio of HEWL to Tetra-P (Fig. 6, *A–C*, *lower panels*). These data were roughly fitted to a single set of binding site models, yielding the thermodynamic parameters (ΔG_{agg}, ΔH_{agg}, and $-T\Delta S_{agg}$, K_D, and n_{agg}) associated with the protein aggregation (Table 2). The parameters (ΔG_{agg}, ΔH_{agg}, and $-T\Delta S_{agg}$) obtained for each titration were plotted against the protein concentrations in the ITC syringe (Fig. 6*D*). The results showed that, in contrast to the binding reaction (Fig. 5*A*), Tetra-P–induced protein aggregation is enthalpy-driven, resulting in the formation of thermodynamically stable aggregates that resist sonication-induced amyloid fibrillation.

The ITC experiments were repeated to evaluate the heat associated with the S-PolyP–induced protein aggregation; the protein solutions at 0.20, 0.35, and 0.49 mM were titrated into S-PolyP solutions of 0.1 mM (Fig. S7) under conditions where protein aggregation is induced (Fig. S8B). The resultant ΔG_{agg}, ΔH_{agg}, and $-T\Delta S_{agg}$ values were plotted in Fig. 6*E*, providing very similar results to those obtained for Tetra-P, representing enthalpy-driven aggregation.

Discussion

In this study, we investigated the amorphous aggregation and fibrillation of HEWL in the presence of polyphosphates under acidic conditions to understand the relationship between the stability and solubility of the protein and its propensity to form amyloid fibrils. The results indicated that the negative charges present in Tetra-P, S-PolyP, and L-PolyP promoted amorphous aggregation of positively charged HEWL, and as the chain lengths of the polyphosphates increased, the concentration required to induce protein aggregation decreased. For these polyphosphates, the data obtained by ITC demonstrated chain length-dependent binding affinity for the protein, consistent with the turbidity data characterizing polyphosphate-induced protein aggregation.

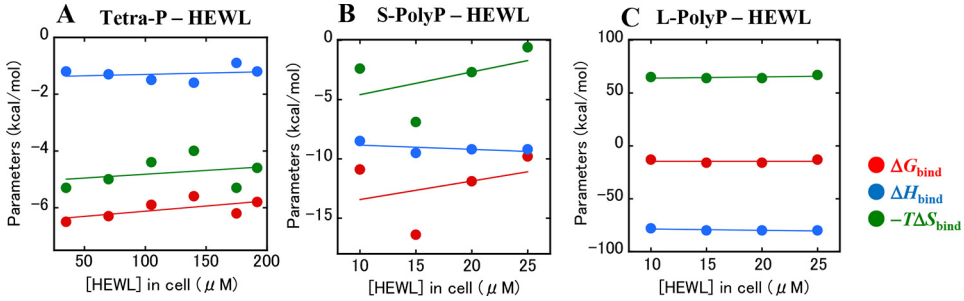

Figure 5. Thermodynamic parameters for the binding of Tetra-P, S-PolyP, and L-PolyP to HEWL. *A*, Tetra-P; *B*, S-PolyP; and *C*, L-PolyP. The values of ΔG_{bind}, ΔH_{bind}, and $-T\Delta S_{bind}$ are plotted against the concentrations of HEWL in the ITC cell. The *solid lines* represent the linear least-squares fit of the data. ITC profiles for the binding of S-PolyP and L-PolyP to HEWL are shown in Fig. S5.

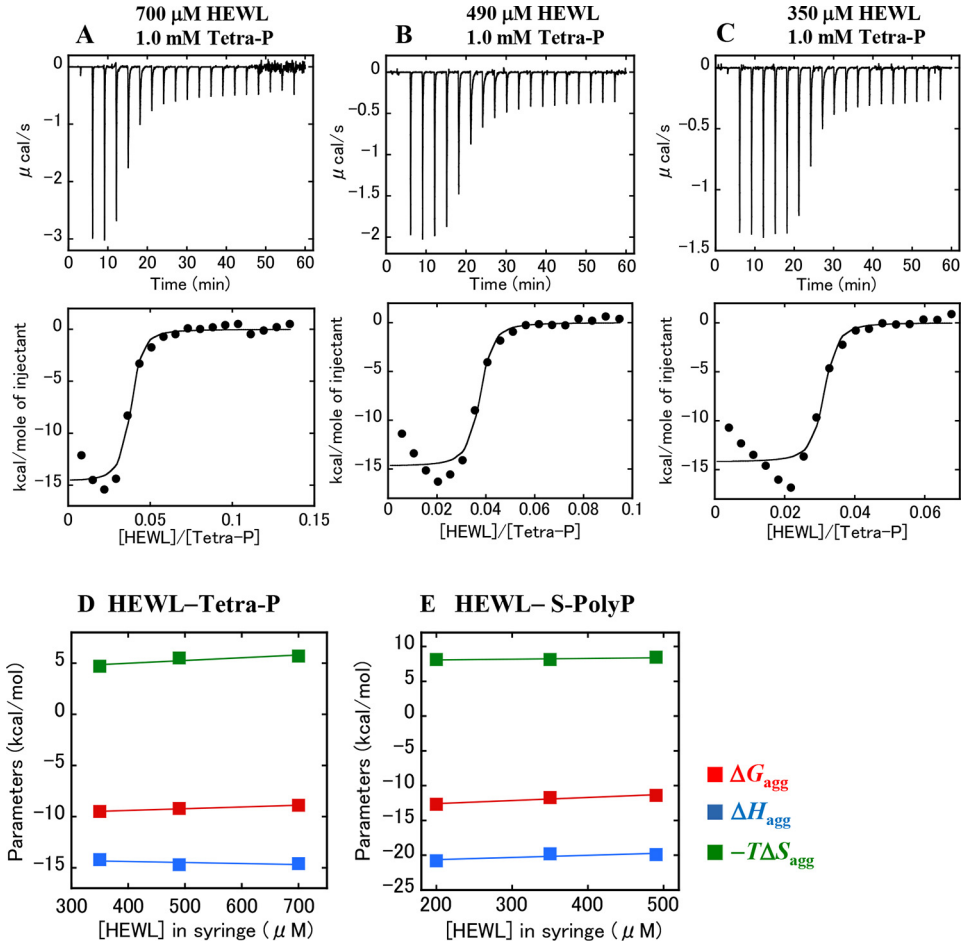

Figure 6. Tetra-P–induced aggregation of HEWL at 25 °C. *A-C*, ITC profiles for the titration of HEWL into the Tetra-P solution. *Upper panels*, raw data for titration. The protein solutions at 700 (*A*), 490 (*B*), and 350 μM (*C*) in the syringe were titrated into the Tetra-P solution at 1.0 mM in the cell. 18 injections of 2 μl were carried out. The final concentrations of HEWL in the cell were 108 (*A*), 75 (*B*), and 54 μM (*C*), and that of Tetra-P was 0.82 mM. *Lower panels*, integrated heat profile of the calorimetric titration shown in the *upper panels*. The integrated heat was plotted against the molar ratio, [HEWL]/[Tetra-P]. The *solid lines* represent the best nonlinear least-squares fit to the single set of binding site models. All the solutions in the syringe and cell contained 10 mM HCl. *D* and *E*, thermodynamic characterization of protein aggregation. The thermodynamic parameters (ΔG_{agg}, ΔH_{agg}, and $-T\Delta S_{agg}$) obtained for protein aggregation induced by Tetra-P (*D*) and S-PolyP (*E*) are plotted against the concentrations of HEWL in the syringe. The *solid lines* represent the linear least-squares fit of the data. ITC profiles for the S-PolyP-induced aggregation of HEWL are shown in Fig. S7.

Interestingly, the calorimetric data indicated that Tetra-P binds to the protein molecules in an entropy-driven process, which is then followed by enthalpy-driven amorphous protein aggregation. As described in the Introduction, regarding the effect of different low-molecular weight salts on protein aggregation, different conclusions have been drawn whether these salts affect protein aggregation primarily through direct protein-salt interactions or indirectly via changes in the structure of water (32–37). In this context, we attribute the entropic contribution upon binding of Tetra-P to protein to the release of hydrated water molecules around the protein surface (44). As shown in studies of the Hofmeister effect (32–34), the phosphate ion is known as a kosmotropic salt, thought to be a "water structure maker." Thus, our results suggest that when four phosphate ions linked by phosphoanhydride bonds bind to HEWL, they prevent water molecules from forming a hydration

Table 2
Thermodynamic parameters associated with Tetra-P-induced protein aggregation at 25 °C

HEWL in the syringe[a]	K_D	n_{agg}	ΔG_{agg}	ΔH_{agg}	$-T\Delta S_{agg}$
	nM			*kcal/mol*	
350	102 (±90)	0.030 (±0.001)	−9.5	−14.2 (±1.0)	4.7
490	171 (±118)	0.035 (±0.001)	−9.2	−14.7 (±0.9)	5.5
700	294 (±166)	0.035 (±0.001)	−8.9	−14.6 (±0.8)	5.7

[a] The concentration of Tetra-P in the cell was 1.0 mM.

structure at the protein surface due to their synergistic kosmotropic effect. At high ratios of Tetra-P to HEWL, the dehydration and resultant structural destabilization of the protein molecules induced by Tetra-P could decrease protein solubility and accelerate protein unfolding, eventually leading to protein aggregation.

As shown in Fig. 5, *B* and *C*, the binding reactions of S-PolyP and L-PolyP to HEWL were enthalpy-favored, indicating a change in binding mode from entropy to enthalpy favored with an increase in polyphosphate chain length. It is noteworthy that large ΔH_{bind} values were observed for the binding of L-PolyP to the protein, indicating that the effect of stronger electrostatic attractions between polyphosphate and HEWL becomes more significant for overall binding as the chain length increase. Thus, it is presumed that the enthalpy effect arising from the stronger electrostatic attraction becomes predominant over the dehydration effect described above with the increase in polyphosphate chain length.

As polyphosphate chain length increases, its interactions with HEWL seem to become more complex. For example, we observed that enthalpy-driven protein aggregation is induced when a small amount of protein solution was titrated into the solutions of Tetra-P and S-PolyP (Fig. 6, *D* and *E*). However, it was difficult to observe the binding-like aggregation with ITC when the protein solution was titrated into the longer L-PolyP solution, probably due to the generation of larger ΔH values of binding and aggregation (data not shown). Furthermore, as shown in Fig. 2, *C* and *D*, the initial increases in turbidity were observed when NaCl was added to the protein solutions containing S-PolyP and L-PolyP. Although a detailed mechanism for this increase in turbidity is not clear, local structural changes of HEWL upon binding of these polyphosphates may affect solution turbidity.

Additionally, as shown in Fig. 1, *C* and *D*, the turbid solutions containing Tetra-P (1 mM) became transparent upon addition of NaCl at 0.3–0.4 M. We conducted the experiments using HEWL at three different concentrations: 0.1, 0.2, and 1.0 mg/ml (data not shown for the protein at 0.1 mg/ml), and all the turbid solutions became transparent when the concentration of NaCl reached 0.3–0.4 M. These results suggest that electrostatic attraction between Tetra-P (1.0 mM) and HEWL (0.1–1.0 mg/ml), which affects protein aggregation, may be saturated under these conditions.

In Fig. 7*A*, we present a plausible model for the aggregation-promoting effect of Tetra-P. In this model, Tetra-P–induced aggregation of HEWL occurs in two successive steps: 1) binding of Tetra-P to HEWL induces dehydration and subsequent structural destabilization of the protein molecules, and 2) as the molar ratio of Tetra-P to HEWL increases, the dehydrated and partially unfolded proteins are stabilized by forming intermolecular associations (*i.e.* aggregation). As indicated by the calorimetric data in Table 2, the stoichiometry (n_{agg}) associated with the Tetra-P–induced protein aggregation was 0.030–0.035, values roughly independent of the HEWL–Tetra-P ratios studied. This result suggests that the electrostatic binding of Tetra-P to the protein and/or aggregates significantly modulates Tetra-P–induced aggregation, in accordance with the structural recovery upon addition of NaCl, as shown in Fig. 3*B*. We suggest that this model is practically applicable to polyphosphates with longer chains, based on the data in Fig. 2 in which S-PolyP and L-PolyP induced very similar aggregation behaviors to those induced by Tetra-P, although the binding mode changes depending on the chain length of polyphosphate (Fig. 5).

Recent *in vitro* studies have shown that additives such as ligands and antibodies, which bind selectively to globular proteins, substantially decrease the propensity for aggregation by inhibiting the global or local unfolding of the protein (45–47). Camelid heavy chain antibody fragments, for instance, have been shown to inhibit the aggregation of amyloidogenic variants of human lysozyme (47). The calorimetric data for Tetra-P–induced aggregation of HEWL presented here suggest that dehydration of the protein upon binding of Tetra-P is a crucial factor for aggregation, in which enthalpy-driven aggregation compensates for entropy-driven binding between the protein and Tetra-P. The relatively high ionic strength *in vivo* where sodium, potassium, and chloride ions as well as charged biomolecules are found has been shown to significantly influence the aggregation of proteins (32–37). In the present study, we showed a combination effect of a simple salt (*i.e.* NaCl) and polyphosphates on HEWL aggregation. The coexistence of two types of salts did not show additive aggregation effects under the conditions used; NaCl played a role in shielding of the electrostatic attraction between HEWL and polyphosphates, indicating an intricate ionic strength dependence on protein aggregation. This finding provides insight into the molecular mechanism of protein aggregation in solutions containing different salts, including polyanions.

To illustrate the effects of Tetra-P and NaCl on amyloid fibrillation of HEWL, a simple phase diagram was constructed (Fig. 7*B*), based on data obtained in this study (Fig. 1, *C* and *E*, and Fig. S2, *A*–*D*). The phase diagram represents conformational states of the protein, which depend on the concentrations of Tetra-P and NaCl. In the absence of NaCl, a strong electrostatic attraction between the positively charged protein and negatively charged Tetra-P induces amorphous aggregation. The addition of NaCl attenuates and ultimately suppresses the interactions causing the protein to aggregate, indicating that they are essentially electrostatic in nature. Near the protein solubility limit in the presence of 0.3–0.4 M NaCl, where the

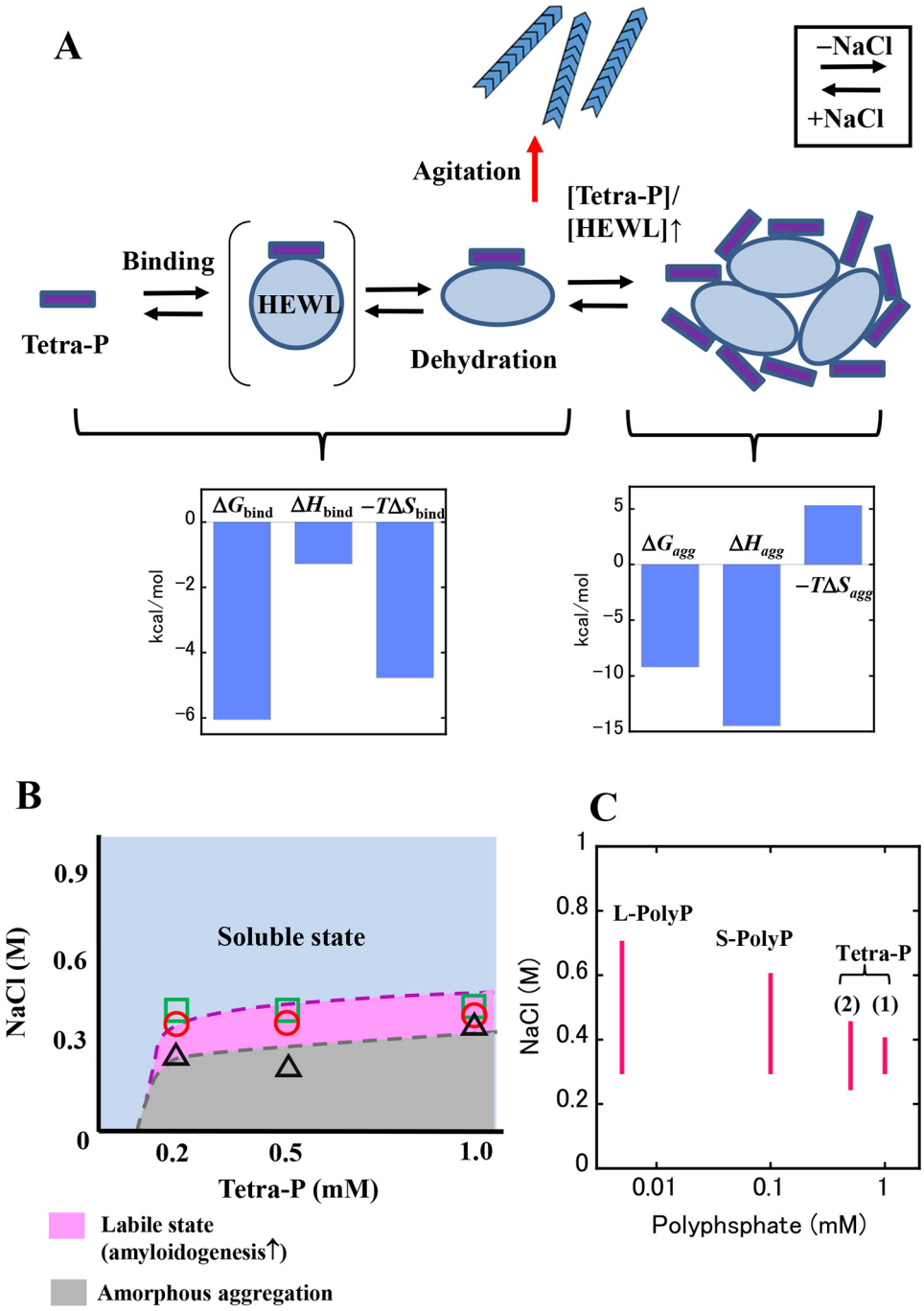

Figure 7. Schematic model for Tetra-P–induced aggregation of HEWL. *A*, schematic showing binding of Tetra-P to HEWL and subsequent protein aggregation. The state in *parentheses* represents the transient binding of Tetra-P to HEWL prior to structural destabilization of the protein. The Tetra-P–bound, destabilized protein is represented by the *elliptical* shape. Protein aggregation is accelerated with an increasing molar ratio [Tetra-P]/[HEWL]. Aggregation states of HEWL shift to a soluble form upon addition of NaCl. Tetra-P–bound protein molecules in labile states have a high propensity to convert into fibrillar structures by agitation. Relationship among the thermodynamic parameters (ΔG, ΔH, and $-T\Delta S$) obtained for the binding reaction and protein aggregation are shown, in which values averaged for each titration are used. *B*, conformational phase diagram of HEWL (1.0 mg/ml) in solutions containing 10 mM HCl, Tetra-P, and NaCl. Soluble, labile, and amorphous aggregation states of HEWL are shown depending on the concentrations of Tetra-P and NaCl. The *circles* represent the critical concentrations of Tetra-P at which protein solutions start to become turbid (Fig. 1*C* and Fig. S2, *A* and *C*). The *squares* and *triangles* demarcate the high and low boundaries of NaCl concentrations, respectively, at which ThT fluorescence was significantly increased by sonication (Fig. 1*E* and Fig. S2, *B* and *D*). *C*, estimated ranges of the labile state. The ranges of labile state of the protein in polyphosphate solutions were estimated from the concentration range of NaCl over which ThT fluorescence was significantly increased by sonication and plotted against the logarithmic concentration of polyphosphate. The data for Tetra-P (*1*) and (*2*) were taken from Fig. 1*F* and Fig. S2*F*, respectively. Those for S-PolyP and L-PolyP were taken from Fig. 2, *E* and *F*, respectively.

protein molecules are in labile states and prone to partial unfolding, fibrillation can be triggered by agitation (Fig. 7*B*). The ranges of the labile state in which the protein molecules are in the soluble states with Tetra-P, S-PolyP, and L-polyP were estimated and shown as a function of the concentrations of polyphosphate (Fig. 7*C*). This result suggests that as the chain length of polyphosphates increased, the labile state of the protein extended over a wider concentration of NaCl. The results

in Fig. 7, *B* and *C*, highlight the propensity of proteins near the solubility limit, modulated by polyphosphates, to convert into amyloid fibrils. Considering that in the highly crowded cytoplasm, many proteins are barely soluble (23, 24), the decreased ability to regulate ion homeostasis with increasing age could be a factor responsible for the late onset of diseases associated with protein aggregation.

Experimental procedures

Materials

HEWL, HCl (1 M), NaCl, Tetra-P, Tri-P, and Pyro-P were purchased from Nacalai Tesque (Kyoto, Japan). S-PolyP and L-PolyP were purchased from Bioenex Inc. (Hiroshima, Japan). The average molecular weights of S-PolyP and L-PolyP were ~1006 and 5153 g/mol. Sodium ion accompanies all the polyphosphates as a counterion. In this study, the molarity of polyphosphate species was used as the phosphate concentration. ThT was obtained from Wako Pure Chemical Industries, Ltd. (Osaka, Japan). HEWL, NaCl, and each polyphosphate were separately dissolved in Milli-Q water. HCl (1 M) was diluted to 100 mM with Milli-Q water. The concentration of HEWL was determined spectrophotometrically at 280 nm with an extinction coefficient of 2.63 ml/mg/cm. Respective solutions were mixed at the desired concentrations. All of the solutions contained 10 mM HCl (pH 2.0).

Turbidity measurements

Turbidity measurements were conducted to detect aggregation of HEWL in the solutions at room temperature. After mixing the solutions for 5 s using a benchtop vortex, the samples were placed into a quartz cuvette (path length of 10 mm). Turbidity values were recorded as the apparent absorption at 600 nm using a Hitachi U3000 spectrophotometer (Hitachi High-Technologies Corporation, Tokyo, Japan).

Detection of amyloid aggregation by sonication

Sonication-induced aggregation of the protein solutions was monitored by measuring the changes in ThT fluorescence using a microplate reader (see Fig. S3).

CD measurements

CD data were obtained with a Jasco 820 spectropolarimeter (Jasco Co., Ltd., Tokyo, Japan) using a quartz cell with a light path of 1 mm. The temperature of the solutions was controlled with a thermoelectrically controlled cell holder attached to the polarimeter. The results were expressed as the mean residue ellipticity after subtracting the buffer baseline. Wavelength-dependent spectra were recorded at 25 °C.

Electron microscopy

A sample solution (5 μl) was placed on a collodion-coated copper grid (Nisshin EM Co., Tokyo, Japan). After incubating for 3 min, the remaining solution was removed with filter paper. The grid was then stained with 0.5% (w/v) hafnium chloride (5 μl) for 1 min. After removing the remaining solution with filter paper, EM images were obtained with a Hitachi H-7650 (Tokyo, Japan) at a voltage of 80 kV.

ITC measurements

Calorimetric experiments were conducted with a PEAQ-ITC instrument (Malvern Instruments, UK) at 25 °C. In the binding experiments, protein solutions in the ITC cell were titrated with polyphosphate solutions in the injection syringe. In the protein aggregation experiments, the polyphosphate solutions in the cell were titrated with the protein solutions in the syringe. Throughout the calorimetric experiments, 18 successive injections (injection volume, 2.0 μl) were performed with intervals of 180 s, and the cell was continuously stirred at 750 rpm. The thermodynamic parameters were determined from the integrated heat using the single set of binding site model supplied by Malvern Instruments. All the sample solutions were prepared in 10 mM HCl.

Author contributions—K. S. conceptualization; K. S. formal analysis; K. S. and Y. G. funding acquisition; K. S., K. Y., M. S., and Y. G. investigation; K. S. methodology; K. S. and Y. G. project administration.

References

1. Eichner, T., and Radford, S. E. (2011) A diversity of assembly mechanisms of a generic amyloid fold. *Mol. Cell* **43,** 8–18 CrossRef Medline
2. Chiti, F., and Dobson, C. M. (2017) Protein misfolding, amyloid formation, and human disease: a summary of progress over the last decade. *Annu. Rev. Biochem.* **86,** 27–68 CrossRef Medline
3. Riek, R., and Eisenberg, D. S. (2016) The activities of amyloids from a structural perspective. *Nature* **539,** 227–235 CrossRef Medline
4. Bemporad, F., and Chiti, F. (2012) Protein misfolded oligomers: experimental approaches, mechanism of formation, and structure-toxicity relationships. *Chem. Biol.* **19,** 315–327 CrossRef Medline
5. Ke, P. C., Sani, M. A., Ding, F., Kakinen, A., Javed, I., Separovic, F., Davis, T. P., and Mezzenga, R. (2017) Implications of peptide assemblies in amyloid diseases. *Chem. Soc. Rev.* **46,** 6492–6531 CrossRef Medline
6. Arosio, P., Knowles, T. P., and Linse, S. (2015) On the lag phase in amyloid fibril formation. *Phys. Chem. Chem. Phys.* **17,** 7606–7618 CrossRef Medline
7. Kuroda, Y. (2018) Biophysical studies of protein solubility and amorphous aggregation by systematic mutational analysis and a helical polymerization model. *Biophys. Rev.* **10,** 473–480 CrossRef Medline
8. Yoshimura, Y., Lin, Y., Yagi, H., Lee, Y. H., Kitayama, H., Sakurai, K., So, M., Ogi, H., Naiki, H., and Goto, Y. (2012) Distinguishing crystal-like amyloid fibrils and glass-like amorphous aggregates from their kinetics of formation. *Proc. Natl. Acad. Sci. U.S.A.* **109,** 14446–14451 CrossRef Medline
9. Ikenoue, T., Lee, Y.-H., Kardos, J., Yagi, H., Ikegami, T., Naiki, H., and Goto, Y. (2014) Heat of supersaturation-limited amyloid burst directly monitored by isothermal titration calorimetry. *Proc. Natl. Acad. Sci. U.S.A.* **111,** 6654–6659 CrossRef Medline
10. Adachi, M., So, M., Sakurai, K., Kardos, J., and Goto, Y. (2015) Supersaturation-limited and unlimited phase transitions compete to produce the pathway complexity in amyloid fibrillation. *J. Biol. Chem.* **290,** 18134–18145 CrossRef Medline
11. Boatz, J. C., Whitley, M. J., Li, M., Gronenborn, A. M., and van der Wel, P. C. A. (2017) Cataract-associated P23T γD-crystallin retains a native-like fold in amorphous-looking aggregates formed at physiological pH. *Nat. Commun.* **8,** 15137 CrossRef Medline
12. Lebendiker, M., and Danieli, T. (2014) Production of prone-to-aggregate proteins. *FEBS Lett.* **588,** 236–246 CrossRef Medline
13. Souillac, P. O., Uversky, V. N., Millett, I. S., Khurana, R., Doniach, S., and Fink, A. L. (2002) Elucidation of the molecular mechanism during the early events in immunoglobulin light chain amyloid fibrillation: evidence for an off-pathway oligomer at acidic pH. *J. Biol. Chem.* **277,** 12666–12679 CrossRef Medline

14. Gosal, W. S., Morten, I. J., Hewitt, E. W., Smith, D. A., Thomson, N. H., and Radford, S. E. (2005) Competing pathways determine fibril morphology in the self-assembly of β2-microglobulin into amyloid. *J. Mol. Biol.* **351,** 850–864 CrossRef Medline
15. Dusa, A., Kaylor, J., Edridge, S., Bodner, N., Hong, D. P., and Fink, A. L. (2006) Characterization of oligomers during α-synuclein aggregation using intrinsic tryptophan fluorescence. *Biochemistry* **45,** 2752–2760 CrossRef Medline
16. Miti, T., Mulaj, M., Schmit, J. D., and Muschol, M. (2015) Stable, metastable, and kinetically trapped amyloid aggregate phases. *Biomacromolecules* **16,** 326–335 CrossRef Medline
17. Annunziata, O., Payne, A., and Wang, Y. (2008) Solubility of lysozyme in the presence of aqueous chloride salts: common-ion effect and its role on solubility and crystal thermodynamics. *J. Am. Chem. Soc.* **130,** 13347–13352 CrossRef Medline
18. Chiti, F., and Dobson, C. M. (2009) Amyloid formation by globular proteins under native conditions. *Nat. Chem. Biol.* **5,** 15–22 CrossRef Medline
19. Auer, S. (2017) Simple model of the effect of solution conditions on the nucleation of amyloid fibrils. *J. Phys. Chem. B* **121,** 8893–8901 CrossRef Medline
20. Bellotti, V., and Chiti, F. (2008) Amyloidogenesis in its biological environment: challenging a fundamental issue in protein misfolding diseases. *Curr. Opin. Struct. Biol.* **18,** 771–779 CrossRef Medline
21. Pace, C. N., Grimsley, G. R., and Scholtz, J. M. (2009) Protein ionizable groups: p*K* values and their contribution to protein stability and solubility. *J. Biol. Chem.* **284,** 13285–13289 CrossRef Medline
22. Adachi, M., Noji, M., So, M., Sasahara, K., Kardos, J., Naiki, H., and Goto, Y. (2018) Aggregation-phase diagrams of β2-microglobulin reveal temperature and salt effects on competitive formation of amyloids *versus* amorphous aggregates. *J. Biol. Chem.* **293,** 14775–14785 CrossRef Medline
23. Ciryam, P., Tartaglia, G. G., Morimoto, R. I., Dobson, C. M., and Vendruscolo, M. (2013) Widespread aggregation and neurodegenerative diseases are associated with supersaturated proteins. *Cell Rep.* **5,** 781–790 CrossRef Medline
24. Ciryam, P., Kundra, R., Morimoto, R. I., Dobson, C. M., and Vendruscolo, M. (2015) Supersaturation is a major driving force for protein aggregation in neurodegenerative diseases. *Trends Pharmacol. Sci.* **36,** 72–77 CrossRef Medline
25. So, M., Hall, D., and Goto, Y. (2016) Revisiting supersaturation as a factor determining amyloid fibrillation. *Curr. Opin. Struct. Biol.* **36,** 32–39 CrossRef Medline
26. Calamai, M., Kumita, J. R., Mifsud, J., Parrini, C., Ramazzotti, M., Ramponi, G., Taddei, N., Chiti, F., and Dobson, C. M. (2006) Nature and significance of the interactions between amyloid fibrils and biological polyelectrolytes. *Biochemistry* **45,** 12806–12815 CrossRef Medline
27. Motamedi-Shad, N., Monsellier, E., and Chiti, F. (2009) Amyloid formation by the model protein muscle acylphosphatase is accelerated by heparin and heparan sulfate through a scaffolding-based mechanism. *J. Biochem.* **146,** 805–814 CrossRef Medline
28. Liu, C., and Zhang, Y. (2011) Nucleic acid-mediated protein aggregation and assembly. *Adv. Protein Chem. Struct. Biol.* **84,** 1–40 CrossRef Medline
29. Motamedi-Shad, N., Garfagnini, T., Penco, A., Relini, A., Fogolari, F., Corazza, A., Esposito, G., Bemporad, F., and Chiti, F. (2012) Rapid oligomer formation of human muscle acylphosphatase induced by heparan sulfate. *Nat. Struct. Mol. Biol.* **19,** 547–554, S1–S2 Medline
30. Cremers, C. M., Knoefler, D., Gates, S., Martin, N., Dahl, J. U., Lempart, J., Xie, L., Chapman, M. R., Galvan, V., Southworth, D. R., and Jakob, U. (2016) Polyphosphate: a conserved modifier of amyloidogenic processes. *Mol. Cell* **63,** 768–780 CrossRef Medline
31. Nitani, A., Muta, H., Adachi, M., So, M., Sasahara, K., Sakurai, K., Chatani, E., Naoe, K., Ogi, H., Hall, D., and Goto, Y. (2017) Heparin-dependent aggregation of hen egg-white lysozyme reveals two distinct mechanisms of amyloid fibrillation. *J. Biol. Chem.* **292,** 21219–21230 CrossRef Medline
32. Bye, J. W., and Falconer, R. J. (2013) Thermal stability of lysozyme as a function of ion concentration: a reappraisal of the relationship between the Hofmeister series and protein stability. *Protein Sci.* **22,** 1563–1570 CrossRef Medline
33. Zhang, Y., and Cremer, P. S. (2010) Chemistry of Hofmeister anions and osmolytes. *Annu. Rev. Phys. Chem.* **61,** 63–83 CrossRef Medline
34. Baldwin, R. L. (1996) How Hofmeister ion interactions affect protein stability. *Biophys. J.* **71,** 2056–2063 CrossRef Medline
35. Arakawa, T., and Timasheff, S. N. (1982) Preferential interactions of proteins with salts in concentrated solutions. *Biochemistry* **21,** 6545–6552 CrossRef Medline
36. Raman, B., Chatani, E., Kihara, M., Ban, T., Sakai, M., Hasegawa, K., Naiki, H., Rao, ChM., and Goto, Y. (2005) Critical balance of electrostatic and hydrophobic interactions is required for β2-microglobulin amyloid fibril growth and stability. *Biochemistry* **44,** 1288–1299 CrossRef Medline
37. Zhou, H. X., and Pang, X. (2018) Electrostatic interactions in protein structure, folding, binding, and condensation. *Chem. Rev.* **118,** 1691–1741 CrossRef Medline
38. Zhang, C.-M., Yamaguchi, K., So, M., Sasahara, K., Ito, T., Yamamoto, S., Narita, I., Kardos, J., Naiki, H., and Goto, Y. (2019) Possible mechanisms of polyphosphate-induced amyloid fibril formation of β_2-microglobulin. *Proc. Natl. Acad. Sci. U.S.A.* **116,** 12833–12838 CrossRef Medline
39. Swaminathan, R., Ravi, V. K., Kumar, S., Kumar, M. V., and Chandra, N. (2011) Lysozyme: a model protein for amyloid research. *Adv. Protein Chem. Struct. Biol.* **84,** 63–111 CrossRef Medline
40. Sasahara, K., Yagi, H., Naiki, H., and Goto, Y. (2007) Heat-induced conversion of β2-microglobulin and hen egg-white lysozyme into amyloid fibrils. *J. Mol. Biol.* **372,** 981–991 CrossRef Medline
41. Kumble, K. D., and Kornberg, A. (1995) Inorganic polyphosphate in mammalian and tissues. *J. Biol. Chem.* **270,** 5818–5822 CrossRef Medline
42. Albi, T., and Serrano, A. (2016) Inorganic polyphosphate in the microbial world. Emerging roles for a multifaceted biopolymer. *World J. Microbiol. Biotechnol.* **32,** 27 CrossRef Medline
43. Gray, M. J., Wholey, W. Y., Wagner, N. O., Cremers, C. M., Mueller-Schickert, A., Hock, N. T., Krieger, A. G., Smith, E. M., Bender, R. A., Bardwell, J. C., and Jakob, U. (2014) Polyphosphate is a primordial chaperone. *Mol. Cell* **53,** 689–699 CrossRef Medline
44. Bagchi, B. (2005) Water dynamics in the hydration layer around proteins and micelles. *Chem. Rev.* **105,** 3197–3219 CrossRef Medline
45. Ray, S. S., Nowak, R. J., Brown, R. H., Jr, and Lansbury, P. T., Jr. (2005) Small-molecular-mediated stabilization of familial amyotrophic lateral sclerosis-linked superoxide dismutase mutants against unfolding and aggregation. *Proc. Natl. Acad. Sci. U.S.A.* **102,** 3639–3644 CrossRef Medline
46. Soldi, G., Plakoutsi, G., Taddei, N., and Chiti, F. (2006) Stabilization of a native protein mediated by ligand binding inhibits amyloid formation independently of the aggregation pathway. *J. Med. Chem.* **49,** 6057–6064 CrossRef Medline
47. Dumoulin, M., Last, A. M., Desmyter, A., Decanniere, K., Canet, D., Larsson, G., Spencer, A., Archer, D. B., Sasse, J., Muyldermans, S., Wyns, L., Redfield, C., Matagne, A., Robinson, C. V., and Dobson, C. M. (2003) A camelid antibody fragment inhibits the formation of amyloid fibrils by human lysozyme. *Nature* **424,** 783–788 CrossRef Medline